Mapping and Localization in Unknown Underwater Electric Field Using Passive Electric Sense System

Penghang Shuai, Haipeng Li, Chao Zhou, *Senior Member, IEEE*, Yaming Ou, *Graduate Student Member, IEEE*, Zhuoliang Zhang, Chunhui Zhu, and Junfeng Fan, *Senior Member, IEEE*

***Abstract*— In nature, some fish species are sensitive to electric fields and these fish are called weakly electric fish. Inspired by the ability of weakly electric fish, this article presents a passive electric sense system for freely swimming underwater robot, and realizes electric field mapping and localization. First, we present the characteristics of underwater electric field, and express these in Maxwell's equations. Then, a Gaussian process (GP)-based approach for interpolation and extrapolation of the underwater electric field is derived, and this approach is embedded with underwater electric field characteristics. This interpolation method is capable of mapping the electric field within the environment, and we can obtain information about the unknown electric field. Finally, based on the electric field maps we constructed, we propose a method for 2-D electro-localization of underwater robot, which is able to fuse multiple constructed electric field maps of different frequencies. In the water environment with unknown electric field emitters, an underwater robot with the passive electric sense system is used for mapping and localization experiments. The experimental results demonstrate the effectiveness of our electro-localization method, and extend the application to unknown electric field sources by mapping method.**

***Index Terms*— Electric field, Gaussian process (GP), localization, mapping, passive electric sense, underwater robot.**

I. Introduction

NATURAL fish have prominent swimming abilities and amazing adaptations in underwater environment. In turbulent flow, fish have multimodal senses to adapt turbid environment that allows navigation, defense, or other biological behaviors. Until now, an increasing number of studies have revealed these wonderful perceptions of fish, such as vision [1], lateral line [2], and electric sense [3]. In order to improve the performance of underwater robot, man-built underwater perception system is essential [4], [5].

Received 10 September 2024; revised 8 November 2024; accepted 6 December 2024. Date of publication 7 March 2025; date of current version 24 March 2025. This work was supported by the National Natural Science Foundation of China under Grant 62033913, Grant 62003341, and Grant 62203436. The Associate Editor coordinating the review process was Dr. Jing Yuan. *(Corresponding authors: Haipeng Li; Chao Zhou.)*

Penghang Shuai is with the Laboratory of Cognition and Decision Intelligence for Complex Systems, Institute of Automation, Chinese Academy of Sciences, Beijing 100190, China, and also with the School of Artificial Intelligence, University of Chinese Academy of Sciences, Beijing 100049, China (e-mail: shuaipenghang2022@ia.ac.cn).

Haipeng Li, Chao Zhou, Yaming Ou, Zhuoliang Zhang, Chunhui Zhu, and Junfeng Fan are with the Laboratory of Cognition and Decision Intelligence for Complex Systems, Institute of Automation, Chinese Academy of Sciences, Beijing 100190, China (e-mail: haipeng.li@ia.ac.cn; chao.zhou@ia.ac.cn; ouyaming2021@ia.ac.cn; zhuoliang.zhang@ia.ac.cn; zhuchunhui2020@ia.ac.cn; junfeng.fan@ia.ac.cn).

Digital Object Identifier 10.1109/TIM.2025.3548185

Electroreception is a special sensory ability, which refers to the ability of creatures to perceive weak electrical signal. Natural electroreception can be considered a part of multimodal haptic sense, by which the weakly electric fish can "grasp" electric fields even in turbid and dark waters [6]. Electroreception can be divided into two forms: the active electric sense and the passive electric sense [7]. The active means weakly electric fish can generate weakly electric field around bodies, that fish have electric organs (EOs) to generate weakly electric field through repetitive discharges (EODs). The self-generated electric field can polarize nearby objects, then the polarized objects distort original electric field. The weakly electric fish can sense the subtle distortion amazingly and extract information relative to the nature, shape, and location of polarized object. This perception is not limited by harsh environment, and weakly electric fish are often found in turbid or dark waters. The African weakly electric fish *Gnathonemmus petersii* inhabited in muddy waters can generate weakly electric field, which utilize sensitive electroreceptors to prey and communicate with others [8]. In nature fish, the most extended electric sense form is passive sense. Fish with passive electric sense can evaluate electric signals emitted by external electric sources, also receive from polarized objects. Even without EO, some fish can possess passive electric sense ability. For example, sharks [9] have electroreceptors, Ampullae of Lorenzini, to detect electric fields with a threshold of sensitivity as low as 5 nV/cm, by which sharks can detect tiny electrical impulses generated by the muscle contractions of nearby fish.

Until now, some studies have focused on underwater artificial electric sense systems. Solberg et al. [3] designed a symmetrically arranged electric fields emission–reception array, where object would cause distortion in the internal electric fields. Solberg et al. [3] developed a particle filter-based method to locate spherical objects within the electric fields. In the active electric field sense domain, Boyer et al. [11] conducted extensive work with "Slender probes" robot designed by them. They achieved object estimation of ellipsoidal target surrounding the underwater robot [10], navigation [11], and wall tracking [12]. Passive electric field sense system typically involve external electrodes for emitting electric field outside underwater robot. Boyer et al. [13] transformed the perception mode of "Slender probes" into passive electric field sense by utilizing electric fields emitted by external electrodes and successfully accomplished navigation task moving toward electrodes. Although satisfactory results have emerged in the

domain of electric field sense, most previous studies focused on rail-driven robots and estimating object targets tasks. However, in recent years, Zheng et al. [14], [15] incorporated passive electric sense system into freely swimming underwater robot maneuvered by propellers. They demonstrated that, with both single and multiple electric field emitters, it is potential to estimate position and orientation of underwater robot using passive electric sense [14], [15].

The aforementioned studies about underwater robots all applied artificially electric fields, which limits the applications of passive electric field. In fact, there are some nature electric fields in the ocean, such as the self-potential [16] generated by minerals being eroded by the ocean and the shaft-rate electric field [17] generated by ships in seawater. It is worth mentioning that the frequency of the ship shaft-rate electric field is consistent with the rotation frequency of propellers. The work done by Zheng et al. [14], [15] is very inspiring but the localization method they used relies on prior knowledge of external electric field emitter, requiring prior knowledge of emission voltage, coordinate positions, and distance between electrodes. However, there are natural electric fields for which it is difficult to obtain prior knowledge. If these unknown electric fields can be detected and utilized, passive electric sense systems can have a wider range of applications.

Moving robot can measure the strengths of field on the trajectory through sensors [18]. However, it is difficult for robot to cover all positions in a large exploration space. A possible approach worth considering is to predict the values that robots have not been reached. Gaussian process (GP) is powerful tool for Bayesian nonparametric inference and learning, providing a framework for fusing first-principles prior knowledge with noisy data [19]. This has made it popular to interpolate and expand the measured physical field, such as magnetic field [20] and high-latitude electric field [21]. Wahlström et al. [22] considered the curl-free properties of the magnetic field, using Maxwell's equations as GP priors, to interpolate the indoor magnetic field. Liu et al. [23] realized indoor magnetic field-based localization with GP Regression (GPR) for magnetic field reconstruction. The integration with prior physical knowledge makes GP credible in results of interpolating physical field, which has frequently been used in modeling and interpolating magnetic field. But to the best of our current knowledge, GP is less used for modeling and interpolation of underwater electric field based on Maxwell's equations as well. Based on our observations, GP is potential tool for underwater electric field reconstruction through passive electric sense.

Inspired by the above observations, this article aims to present a method to extract underwater electric field information in a region, and expand the robot localization scenarios to unknown prior parameters about electric field sources for freely swimming underwater robot. For the underwater electric fields we are interested in, we present their physical properties. Embedded with the physical knowledge of the electric field, a GP-based approach is introduced for underwater electric field mapping under unknown prior information about sources scenarios. From the comprehensive information of electric field maps, we propose a robot localization algorithm based on constructed electric field maps, which enables precise localization of underwater robot in the unknown electric field sources situation. Furthermore, we assess the efficacy of the localization method using maps containing more electric field sources. The contributions of this article are summarized as follows.

1) This work proposes a mapping method for unknown underwater electric field, which is embedded with physical knowledge to interpolate and extrapolate underwater electric field from measurement data.
2) This article introduces an localization approach that, by utilizing the electric field maps without prior parameters about electric field sources, accomplishes the electro-localization task for freely swimming underwater robot.

The rest of this article is organized as follows. Section II explores the characteristics of underwater electric fields and the implicit information. Section III introduces electric field mapping algorithm we designed, and particle filter-based algorithm for robot localization task. Section IV describes the freely swimming underwater robot equipped passive electric sense system that we designed for experiments. Section V introduces the experiment of constructing electric field maps and the robot localization. Finally, the conclusion and the future work are summarized in Section VI.

II. Characteristics Analysis of Underwater Electric Field

To the best of our knowledge, in previous works when underwater robots were considering to exploit information about electric field in the environment, they always rely on accurate modeling of the electric field, which requires sufficient prior information. This shortcoming limits the application of electric sense to underwater robots. In our previous introduction, we have mentioned that there are a large number of low-frequency natural electric fields in the ocean, it is meaningful to look for common characteristics of these fields, which can be potential basis for the reconstruction of underwater electric field.

The origin and coupling propagation of the electromagnetic field in medium are fully described by Maxwell's equations (1), which suitable for all electromagnetic fields. In (1), time-varying magnetic field $\mathbf{H}$ affects electric field $\mathbf{E}$, also time-varying electric field affects magnetic field. Besides, the propagation of electromagnetic field in medium is influenced by the permittivity ε, permeability μ and conductivity σ. Among this, we can learn that the electric field is affected by many factors

$$\begin{cases} \nabla \times \mathbf{E} = -\mu \dfrac{\partial \mathbf{H}}{\partial t} \\ \nabla \times \mathbf{H} = \sigma \mathbf{E} + \varepsilon \dfrac{\partial \mathbf{E}}{\partial t} \\ \nabla \cdot \varepsilon \mathbf{E} = \rho \\ \nabla \cdot \mu \mathbf{H} = 0. \end{cases} \tag{1}$$

Electric field is a kind of special electromagnetic wave when it propagates in the water medium. According to (1), the current of propagation in the medium can be divided

into conduction current $\mathbf{J}_c = \sigma\mathbf{E}$ and displacement current $\mathbf{J}_d = \varepsilon(\partial\mathbf{E}/\partial t)$. In this article, the mentioned underwater electric fields are low-frequency. When the frequency of electric field is low and propagates in the water, displacement current can be neglected, leaving the electromagnetic field as electroquasistatic case [24]. To describe the relationship between frequency and electroquasistatic field, the ratio of displacement current to conduction current is expressed as follows:

$$\frac{\mathbf{J}_d}{\mathbf{J}_c} = \frac{\varepsilon}{\sigma}\omega \ll 1 \tag{2}$$

where ω is the angular frequency. When the ratio of displacement current and conduction current satisfies (2), the electromagnetic wave can be regarded as quasi-static electric field underwater, that displacement current can be neglected. According to Momma's calculation [24], displacement current can be ignored when the frequency of the electric field propagating in fresh water is less than several MHz that several hundred MHz in seawater. The frequency of the electric field involved in this article is much lower than 1 MHz, so it is can be regarded as electroquasistatic field. Based on this case, Maxwell's equations can be simplified to the following form:

$$\begin{cases} \nabla \times \mathbf{E} = 0 \\ \nabla \times \mathbf{H} = \sigma\mathbf{E} \\ \nabla \cdot \varepsilon\mathbf{E} = \rho \\ \nabla \cdot \mu\mathbf{H} = 0. \end{cases} \tag{3}$$

Moreover, the Maxwell's equations in the electroquasistatic case mainly modify the description of the curl of electric field and magnetic field. In this case, the curl of electric field is always zero, not coupled with time-varying magnetic field, while the curl of magnetic field is only related to displacement current, reducing the degree of coupling between magnetic and electric field. Therefore, when measuring underwater electric fields in quasi-static condition, it is not necessary to consider influence from surrounding electric field generated by time-varying magnetic field in the environment and regarded these electric field as curl-free.

Specifically, when the electric source emitted electric field is electric dipole which formed by positive and negative charges, these field is always curl-free field. Even without considering the frequency of the electric field generated by electric dipole, the field must be curl-free [25]. Fig. 1 illustrates our analysis of underwater electric field characteristics, which is considered to be curl-free in the exploring region.

From previous analysis, we have known the common feature is curl-free for low-frequency natural electric fields in the ocean, while their divergences still depend on a prior knowledge of the field source. In order to apply electric sense for underwater robot, we aim to extract more information from the electric field. According to electrodynamics, the electric field is superpositional, therefore, the electric field applied to a point $\mathbf{P}$ is the vector sum of all the surrounding electric fields. The strength of electric field at point $\mathbf{P}$ can be expressed as follows:

$$\mathbf{E}(\mathbf{P}) = \sum_i \frac{\mathbf{Q}_i \mathbf{r}_i}{4\pi\sigma r_i^3} \tag{4}$$

where assume that the vectorial diameter from the ith charge $\mathbf{Q}_i$ to the point $\mathbf{P}$ is $\mathbf{r}_i$. We can learn that when the position of the measuring point changes, the electric field strength obtained also changes. The relationship makes it possible to use the electric field strength for localization. By reverse mapping this formula, the measured electric field strength at point $\mathbf{P}$ can be used as input for underwater robot localization.

With the curl-free condition for electric field, a common way is to define a scalar potential ϕ to indirectly measure strengths of electric fields. The relationship between the electric field and electric potential can be expressed as

$$\mathbf{E} = -\nabla\phi. \tag{5}$$

The equation indicates that the electric potential field is scalar field. Therefore, in the article, the method of measuring the electric field used is to measure the electric potential through an analog-to-digital converter (ADC).

III. Mapping the Underwater Electric Field and Robot Localization

A. Mapping the Underwater Electric Field Using GP Priors

In Section II, we have analyzed the characteristics of low-frequency underwater electric fields and the potential of electric sense for localization. The construction of electric field map allows to obtain all the electric field information for a underwater area, without involved prior parameters. However, exploration of all area is not possible. This section aims to design a method that it can extrapolate and interpolate the electric field strengths for unreached locations throughout the region, which fuses physical knowledge of underwater electric field.

GP is distribution on real-value function, which is suitable for modeling spatially correlated measurement. GPR is an implementation of the GP, mapping from an input $\mathbf{x}_*$ to predict $f(\mathbf{x}_*)$, by which learning amounts to computing the posterior process with dataset $\mathcal{D} = \{(\mathbf{x}_i, y_i)\}_{i=1}^n$. Normally, this model GPR is written as

$$\begin{aligned} f(\mathbf{x}) &\sim \mathcal{GP}(\mu(\mathbf{x}), \kappa(\mathbf{x}, \mathbf{x}')) \\ y_i &= f(\mathbf{x}_i) + \varepsilon_i \end{aligned} \tag{6}$$

where ε_i is Gaussian noise and $\varepsilon_i \sim \mathrm{N}(0, \sigma^2_{\text{noise}})$. And $\mathbf{x}$ is the position vector where noisy measurement scalar y_i is observed. $\mu(\mathbf{x})$ is mean function of $f(\mathbf{x})$ and $\kappa(\mathbf{x}, \mathbf{x}')$ is covariance function between two locations $(\mathbf{x}, \mathbf{x}')$. Specifically, the covariance function is the crucial component, which encodes the assumptions to be learned. Prediction of input $\mathbf{x}_*$ amounts to the following [19]:

$$\begin{aligned} p(f(\mathbf{x}_*)|\mathcal{D}) &= \mathrm{N}(f(\mathbf{x}_*) \mid \mathbb{E}[f(\mathbf{x}_*)], \mathbb{V}[f(\mathbf{x}_*)]) \\ \mathbb{E}[f(\mathbf{x}_*)] &= \mathbf{k}_*^{\mathsf{T}}\left(\mathbf{K} + \sigma^2_{\text{noise}}\mathbf{I}_n\right)^{-1}\mathbf{y} \\ \mathbb{V}[f(\mathbf{x}_*)] &= \kappa(\mathbf{x}_*, \mathbf{x}_*) - \mathbf{k}_*^{\mathsf{T}}\left(\mathbf{K} + \sigma^2_{\text{noise}}\mathbf{I}_n\right)^{-1}\mathbf{k}_* \end{aligned} \tag{7}$$

where $\mathbf{K}_{i,j} = \kappa(\mathbf{x}_i, \mathbf{x}_j)$, $\mathbf{k}_*$ is an n-dimensional vector with ith element $\kappa(\mathbf{x}_*, \mathbf{x}_i)$, and $\mathbf{y}$ is an n-dimensional vector of observations. The prediction key of GPR is computing the conditional mean $\mathbb{E}[f(\mathbf{x}_*)]$ and variance $\mathbb{V}[f(\mathbf{x}_*)]$ of the

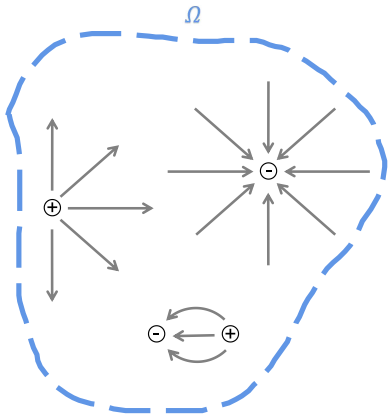

Fig. 1. Illustration of electric fields with zero curl. In this region Ω, there are curl-free electric fields emitted by positive charge, negative charge, and electric dipole.

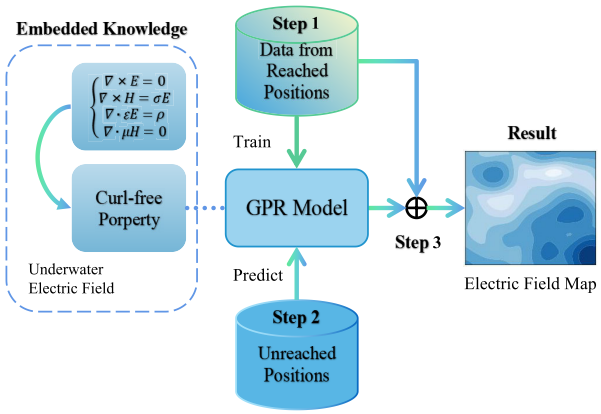

Fig. 2. Framework of mapping method. The GPR model is able to reconstruct the electric field map in region using the collected data. The core of the mapping method is GPR model embedded with curl-free property from model of underwater electric field. First, the data from reached positions are used as input into GPR model to predict the field values in unreached positions. Finally, both of them form the result map.

process evaluated at the test input because both the prior and posterior maintain Gaussianity.

In (6), the mean function $\mu(\mathbf{x})$ often assumed to be $\mu(\mathbf{x}) = 0$ without loss of generality. The covariance function $\kappa(\mathbf{x}, \mathbf{x}')$ contains the relationship between the different measurements, so the choice of it is encompassed prior physical knowledge about the GP. For underwater electric field, as shown in Fig. 1, we have analyzed the time-varying field at low frequency and electric dipole field are curl-free in Section II, and the divergences are related to the charge quantities of sources and remain constant. When measuring the strength of electric field at a position in the region Ω, due to the previous analysis that external time-varying magnetic field cannot affect the electric field under quasi-static condition. Hence, direct measurement of the electric field at a specific position can be considered as resulting from multiple sources. By transforming the original signal into frequency domain, we are capable of discerning the distinct frequencies of electric fields received at a specific position.

The relation (5) and curl-free field (3) are the key that we will utilize in our GPR model of the underwater electric field. Based on (5), the electric field $\mathbf{E}$ can be written as the gradient of scalar potential $\phi(\mathbf{x})$, where $\phi : \mathbb{R}^2 \to \mathbb{R}$ and $\mathbf{x} \in \mathbb{R}^2$ in Cartesian coordinates. Considering curl-free characteristic of underwater electric field above, the GPR model we established is following:

$$\begin{aligned} \phi(\mathbf{x}) &\sim \mathcal{GP}(0, \kappa_{\text{lin.}}(\mathbf{x}, \mathbf{x}') + \kappa_{\text{SE}}(\mathbf{x}, \mathbf{x}')) \\ \mathbf{y}_i &= -\nabla\phi(\mathbf{x}_i) + \varepsilon_i, \quad \varepsilon_i \sim \mathrm{N}\big(\mathbf{0}, \sigma^2_{\text{noise}}\mathbf{I}_3\big) \end{aligned} \tag{8}$$

where the covariance functions are the squared exponential (SE) functions and the linearly *dot product* covariance function

$$\kappa_{\text{SE}}(\mathbf{x}, \mathbf{x}') = \sigma^2_{\text{SE}} \exp\left(-\frac{\|\mathbf{x} - \mathbf{x}'\|^2}{2\ell^2_{\text{SE}}}\right) \tag{9}$$

$$\kappa_{\text{lin.}}(\mathbf{x}, \mathbf{x}') = \sigma^2_{\text{lin.}}\mathbf{x}^{\mathsf{T}}\mathbf{x}'. \tag{10}$$

The covariance functions are typical radial basis functions (RBFs), and can used to be kernels for curl-free vector fields [26].

In model (8), the linear operator nabla (∇), which preserves Gaussianity under linear operations, enables the direct utilization of the derivative measurements in GPR. It should be noted that the electric field involved in this article is periodic and approximately sinusoidal, and after differentiation, these only has phase difference with the original field. Therefore, the measured values ϕ can be equivalently used as GP priors, and the model (8) can be written on the underwater electric field $\mathbf{E}(\mathbf{x})$ as

$$\mathbf{E}(\mathbf{x}) \sim \mathcal{GP}\big(0, \sigma^2_{\text{const.}}\mathbf{I}_3 + \mathbf{K}_{\text{curl}}(\mathbf{x}, \mathbf{x}')\big) \tag{11}$$

where $\mathbf{K}_{\text{curl}}(\mathbf{x}, \mathbf{x}')$ is called curl-free kernel, regarding its construction and application can refer to [26], [27], and [28]. This curl-free kernel ensures that GPR (8) adheres the curl-free constraints of underwater electric field (3). In this model, there are four hyperparameters should be optimized: magnitude scale parameters ($\sigma^2_{\text{const.}}$ and σ^2_{SE}), length-scale parameter (ℓ_{SE}), and noise scale parameter (σ^2_{noise}), and a common method is calculating the negative marginal likelihood function [19]

$$\begin{aligned} \mathcal{L}(\boldsymbol{\theta}) &= -\log p(\mathbf{y} \mid \boldsymbol{\theta}, \mathcal{D}) \\ &= \frac{1}{2}\mathbf{y}^{\top}{\mathbf{K}_{\mathbf{y}}}^{-1}\mathbf{y} + \frac{1}{2}\log|\mathbf{K}_{\mathbf{y}}| + \frac{n}{2}\log 2\pi \end{aligned} \tag{12}$$

where $\mathbf{K}_{\mathbf{y}} = \mathbf{K}_{\theta} + \sigma^2_{\text{const.}}\mathbf{I}_n$ is the covariance matrix, in which $\mathbf{y} \in \mathbb{R}^{2\times n}$ and $\mathbf{K}_{\theta} \in \mathbb{R}^{n\times n}$.

The field mapping method can be summarized by Fig. 2. In conclusion, with the curl-free property of underwater electric field, the GPR model (8) is able to learn the field map from the measured data on robot path and then predict the field data for unreached positions. Finally, the real values from the explored path and the predicted values for the unreached positions together form the electric field map.

B. Localization Method Based on Electric Field Maps

According to our survey, the studies applying passive electric sense to localization of freely swimming underwater robots is scarce, and the localization methods used rely on sufficient prior information of the electric field sources in the environment. The mapping of the electric field allows obtaining electric field information when the electric sources are unknown. We have previously presented a method for constructing map of underwater electric field, moreover,

it demonstrates the potential of using electric field information for freely swimming robot localization. This section aims to design a localization algorithm for our electric sense robotic fish applying constructed electric field maps, and to extend the application scenario of passive electric sense to the case of the unknown information about electric sources.

The previous analysis and model can be succinctly summarized as the construction of electric field map in 2-D region Ω

$$\mathbf{E}_{\text{map}}(\mathbf{x}) = \phi_{\mathbf{x}}, \quad \mathbf{x} \in \Omega. \tag{13}$$

The map takes location $\mathbf{x}$ as input and output electric potential $\phi_{\mathbf{x}}$, which corresponds to the measurement of robot. The process of mapping dose not necessitate measuring the entire region, it leverages existing data to interpolate unexplored sub-regions.

When robot needs to perform tasks, these are normal requirements that knowing the location of robot and providing intuitive visualization for human operator. Usually, the map is required to support other tasks, such as navigation [29] and robot localization [30]. The tradition method of building map is to scan the surrounding environment of the robot through LIDAR and camera. These sensors provide information about the distances and orientations to landmarks, which contains environmental information and implicitly reveals the robot's position. The electric field data from passive electric sense system, similar to these sensors, encompasses the necessary information for mapping based on electric theory. In robotic mapping problem, the fixed electric field emitter can be likened to discernible fixed landmark which detectable through camera and LIDAR. Zheng et al. [14], [15] completed localization and pose estimation tasks based on electric sense, that they built map using the electric theory and prior knowledge about fixed emitter, which method is similar to make environment known. In this article, the construction of electric field map is achieved through the measurement of environment by operator and interpolation for unreached positions in advance. Based on these, we consider that it is a feasible way to undertake underwater robot's localization task by electric field maps.

For our localization task, particle filter method is worthy to consider. As a nonparametric method, particle filter method is common method for robot localization method [31], which does not rely on deterministic posterior function but instead approximates it using finite set of values. Consequently, particle filter avoids the need for strong parametric assumptions regarding the posterior density and effectively captures intricate confidence levels [32]. The relative position between the robotic fish and "electric landmarks," electric field emitters, cannot be directly obtained, but rather indirectly acquired through the probability of location on the maps determined by measured potential values. This idea also aligns with the concept of particle filter, and it focus their particles—the most possible results—on regions in state-space with likelihood [33].

The electric field map we constructed is not one-to-one function, that the electric potential ϕ, scalar value without direction, remains the same at different positions according to the electric theory. When using measurement from a moment to predict the current position of the robot, it is common for multiple positions to converge in the area. Particle filter incorporates information about the previous state of the robot, thereby enhancing prediction reliability.

Algorithm 1 Underwater Robot Localization Using Electric Field Maps

Input: Electric maps $\{\mathbf{E}_{map(i)}(\mathbf{x})\}_{i=1}^{M}$, electric potentials $\{\mathcal{V}_{(t)}\}_{t=1}^{T}$, motion signals $\{u_{(t)}\}_{t=1}^{T}$
Output: Predicted positions of robotic fish $\{\mathbf{x}_{*(\mathbf{t})}\}_{t=1}^{T}$

```
Initialization of N particles and their importance weights:
  {X_0^(i)}_{i=1}^N ~ q(x_0),   {w_0^(i)}_{i=1}^N = 1/N
for k=2,T do
    Update particles:
    {X_k^(i)}_{i=1}^N ~ p(x_k|X_{k-1}^(i), u_{k-1}).
    Update importance weights of particles:
    {w_k^(i)}_{i=1}^N ∝ p(V_t|X_k^(i)) w_{k-1}^(i).
    Normalize particle importance weights:
    w̃_k^(i) = w_k^(i) / Σ_{i=1}^N w_k^(i)
    Resample particles:
    {X_k^j, w_k^j}_{j=1}^N =Resampling({X_k^j, w̃_k^j}_{j=1}^N)
    Estimate current position of robotic fish:
    E[x_*t] = Σ_{i=1}^N X_k^(i) w̃_k^(i)
    if Particles convergence then
        for d=k-1, 1 do
            Estimate backward positions:
            x_*(d) ~ p(x_d|x_*(d+1), -u_d)
        end for
    end if
end for
return {x_*(t)}_{t=1}^T
```

The passive electric sense robotic fish we designed is able to discriminate between electric fields of multiple frequencies and build maps for the different frequencies separately. Therefore, the use of measurements at multiple frequencies also needs to be considered when maps of electric fields at multiple frequencies are involved. For M electric fields of different frequencies, the receiver's measurements after short-time Fourier transform (STFT) are

$$\mathcal{V} = [\phi_1, \ldots, \phi_M]^T. \tag{14}$$

In particle filter, each particle represents a possible result, and the key parameter is the importance weight of particle, which indicates its contribution to the posterior estimation—predicted position of robotic fish in this task. The update of importance weights reflects our understanding of the possible position in maps. The importance weight of the measurement is

$$p\left(\mathcal{V}|\mathcal{X}_k^{(i)}\right) = \frac{1}{\sqrt{2\pi\sigma_m^2}} \exp\left(-\frac{|\sum_{i=1}^{M} l_i \times \left(\mathcal{V}_i - \mathbf{E}_{\text{mapi}}\left(\mathcal{X}_k^{(i)}\right)\right)|^2}{2\sigma_m^2}\right) \tag{15}$$

where l_i is ith linear coefficient for ith electric field map and σ_m is the factor of the importance weight. The goal of the equation is to calculate the difference between the actual measurement and the predicted measurement of the location,

and the merging maps of multiple frequency electric fields is by linear weighted sum.

Specially, the underwater robot localization method requires several steps to converge, and the estimation of the robot's positions is inaccurate before convergence. Expanding upon the basic particle filter algorithm, which is called estimating forward positions, we have integrated estimating backward positions after the particles convergence. Through the previous motion signals and current estimating position obtained after convergence, the estimating backward positions can correct the previous trajectory. The estimating backward positions in terms of algorithm convergence improves the precision of estimating the complete trajectory. The estimating backward positions is 8–12 steps in Algorithm 1. Our localization method is as shown in Algorithm 1, in which the resampling method is low variance sampling [32], [34].

IV. Passive Electric Sense System

A. Passive Electric Sense Robotic Fish

To validate our methods, we have designed a freely swimming robotic fish equipped with passive electric sense system. The robotic fish can perceive the electric field in the water, while operators can control the movement of it through remote controller. The biomimetic robotic shark designed in this article is shown in Fig. 3. The robotic fish, with a total length of 770 mm, is mainly composed of a head compartment and a multijoint tail, of which shell is made by 3-D printed nylon material. Inside the head compartment, there are a receiver circuit for collecting signals from electrodes and a controller circuit (STM32F407) for controlling its swimming mode. The front of the receiver has a low-pass filter and it uses ADS1256 (24 bit), whose measurement range is −5 to 5 V, as the main chip to collect potential values and send real-time data to the remote host computer onshore. The controller can receive control commands from onshore remote controller, allowing operators to control the direction and speed of the robotic fish. The propulsion of the robotic shark relies on multiple servos, with PWM signals sent from the control board to control their angles θ_i. The central pattern generator (CPG) method is employed to achieve various motion modes of our robotic fish, which only requires inputting desired swing amplitude, frequency, and bias.

On the belly of the robotic fish, there are Ag/Agcl electrodes that perceive electric field. In this work, the method of perceiving electric field is using absolute electrode, where is near the head of robot. Ag/Agcl electrodes have good potential stability and are widely used in underwater electric field measurement [35], [36], [37] and electroencephalogram [38]. However, Ag/Agcl electrodes have short lifespan issues. Therefore, this article adopts button-style fastening method (see Fig. 4) to fix external measuring electrodes on fish body where button base connects with internal circuits inside robotic fish, so that when it is necessary to replace electrodes only need replacing Ag/Agcl buttons without changing other parts. Specifically, the female fastener has connected to the receiver in the robotic fish. The Ag/Agcl can be pressed into the male fastener, then it can be easily fastened to the female

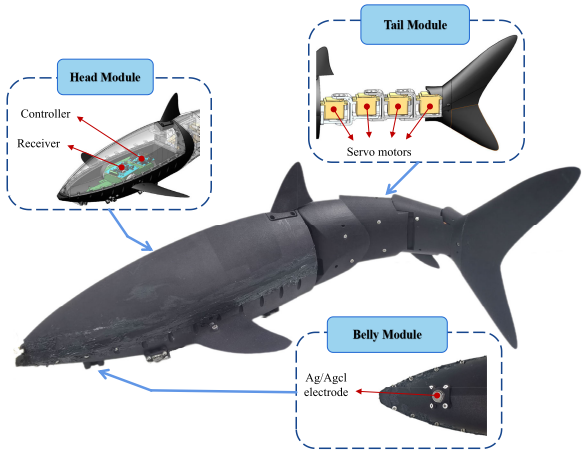

Fig. 3. Prototype of the robotic fish.

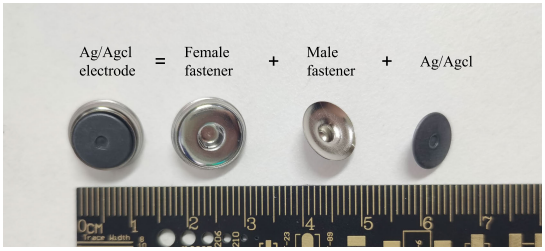

Fig. 4. Prototype of the Ag/Agcl electrode.

fastener in Fig. 4. The design is also commonly used in electroencephalogram.

It is worth stating that in addition to the passive electric field sense system, the robotic fish in this article lacks any other sensory capabilities.

B. Experimental Setup of Passive Electric Sense

To illustrate the ability of our electric sense robotic fish, we have built the experimental scenario in a pool of water. Multiple sine signal generators with varying electric field frequencies are positioned within $5 \times 4 \times 1.2$ m^3 (length × width × height) water tank. Submerged copper electrodes generate an electric field within the tank, while camera situated atop records and stores the robot's positions on an upper computer. For discriminating electric fields of different frequencies in real time, the onshore upper computer is capable of conducting STFT on receiving voltage data to record amplitude information pertaining to changes in the desired frequency range. To address spectral leakage, Hanning window function is employed.

The electric field emitter is buoyant and fixed on the water surface and consists of two copper electrodes enclosed within a square plastic box, which is equipped with two underwater pipes as depicted in Fig. 5. The total length of the emitter measures 380 mm, enabling the generation of electric field at depth approximately 200 mm below the water surface. A direct digital synthesizer (DDS) module is housed inside the plastic box to generate ac signals encompassing diverse waveforms, frequencies, and amplitudes. In Zheng's study, passive electric sense ac-based empowers underwater robot to perceive distant signals [15]. Moreover, if multiple electric field signals are desired to coexist in the water, it only necessitates altering

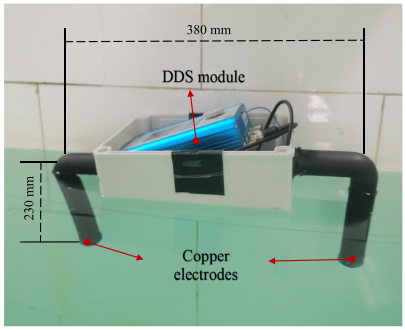

Fig. 5. Electric emitter architecture.

the frequency of each sine signal to establish distinguishable electric fields across the aquatic region.

V. Experiment

A. Experimental Framework

Our experimental framework is shown in Fig. 6. In the experimental pool, there are multiple electric emitters with different frequencies which float on the water and are fixed at three positions. The free swimming robotic fish can measure the electric potential ϕ sampled at 500 Hz, while the camera at the top of pool is recording the position of robot. In all steps, the robotic fish cruise with constant tail oscillation frequency of 0.6 Hz, which allows for the collection of data ϕ from a specific location sufficiently. The measurement data are transmitted to upper computer via Bluetooth, then STFT will be applied to display real-time frequency spectrum images in step 1. In Fig. 6, image of step 1 has shown the frequencies of robotic fish measurement, which clearly demonstrates significant amplitude variations at frequencies of 40, 60, and 70 Hz. Consequently, data at these three frequencies are recorded.

In step 2, the data from step 1 are utilized to generated electric field maps by model (11). The generated maps will be used for the robot's localization task. For our localization task, the robotic fish is controlled in the pool and subsequent measurements are conducted, and the measurement trajectory is presented in Fig. 6. In step 4, we accomplish the localization task by employing underwater robot localization algorithm with the electric field maps acquired in step 2.

B. Mapping the Underwater Electric Field

For our electric sense robotic fish, the electric field in the water is completely unknown, but we aim to build maps of the different frequency electric fields. Before mapping process, the robotic fish needs to extract information about the underwater electric fields. Our law is selecting frequency quantities that have a large change in amplitude as the position of the robot changes in real-time frequency domain. Based on previous analyses of the relationship between electric field strength and position, there is a greater likelihood that the electric field source for these frequency quantities is present in the water to be detected. Fig. 7 shows the frequency domain of two moments at different positions. At 40, 60, and 70 Hz in graph, there are large variations, therefore the amplitudes of these three frequencies are recorded as the training set needed to build the maps.

The experiment is concerned with estimating electric field maps, corresponding to step 2 in Fig. 6. In the previously mentioned experimental setting and the data obtained in step 1, we have acquired the required training set. The upper computer records the training set $\mathcal{D} = \{(\mathbf{x}_i, \mathcal{V}_i)|i = 1, 2, \ldots, t\}$ required by the model (11), where $\mathcal{V}_i$ is amplitude data vector of frequencies recorded at time i, and $\mathbf{x}_i$ is real position of robotic fish from camera. The time complexity of exact GP inference is $\mathcal{O}(n^3)$, where n is the number of data points [19]. Gridding the original map can reduce data volume, this high computational cost can often be circumvented. In this article, we split equally the 2-D image into 45×54 raster map, and we employ model (11) on a personal computer equipped with an Intel i5-12400F 2.5 GHz CPU and 16 GB RAM. The optimized hyperparameters are $\sigma_{\text{lin.}} \approx 0.316$, $\sigma_{\text{SE}} \approx 0.707$, $\ell_{\text{SE}} \approx 10$, and $\sigma_{\text{noise}} \approx 1$.

In experimental pool, three electric field emitters are observed at left, below, and right in fact, corresponding to frequencies of 40, 60, and 70 Hz. The data collection process is controlling the robotic fish to cruise for collecting the electric field information in the region, and the camera on the top of the pool records the position and the corresponding measurement in real time. The sample path for mapping is shown in Fig. 8. The size of the original training dataset is $n = 6555$, and then $n = 951$ in 45×54 raster map. For these inputs, the designed program has took a total of 148.3335 s to complete mapping, which includes 148.1872 s for model training and 0.1463 s for prediction. Three frequency quantities are recorded, corresponding to three electric field emitters. Fig. 9 shows the three interpolated electric fields of GP. In the obtained electric field maps, the darker blues indicates larger magnitudes of maps, and the boundary of the mapping result is the boundary of the explored space. From the mapping results, the variation of the electric field amplitude is not linear. The electric field maps obtained at each frequency can correspond to the actual position of the electric field emitters. In Fig. 9, the areas in maps with the maximum magnitude spread outward in circular shape, which is also consistent with the electric theory.

In this experiment, we have obtained multiple electric field maps at different frequencies. These electric field maps implicitly contain information about the electric field sources, and their strength distributions are consistent with electric field theory. This result shows that our GPR interpolation model is valid.

C. Localization With Electric Field Map

In Sections II and III, we have introduced the theoretical method and experimental setup for building electric field maps, as well as particle filter algorithm used for robot localization. In this section, we continue with the experimental setup and use electric field maps we have generated from step 2 in Fig. 6. In step 3, the underwater robot is controlled to measure the electric field on the path and this data will be used for robot localization task.

The particle filter method used in this experiment takes into the current measured potentials of the robotic fish, as well as the previously measured values. This feature makes it possible to use noninjective functions as localization maps.

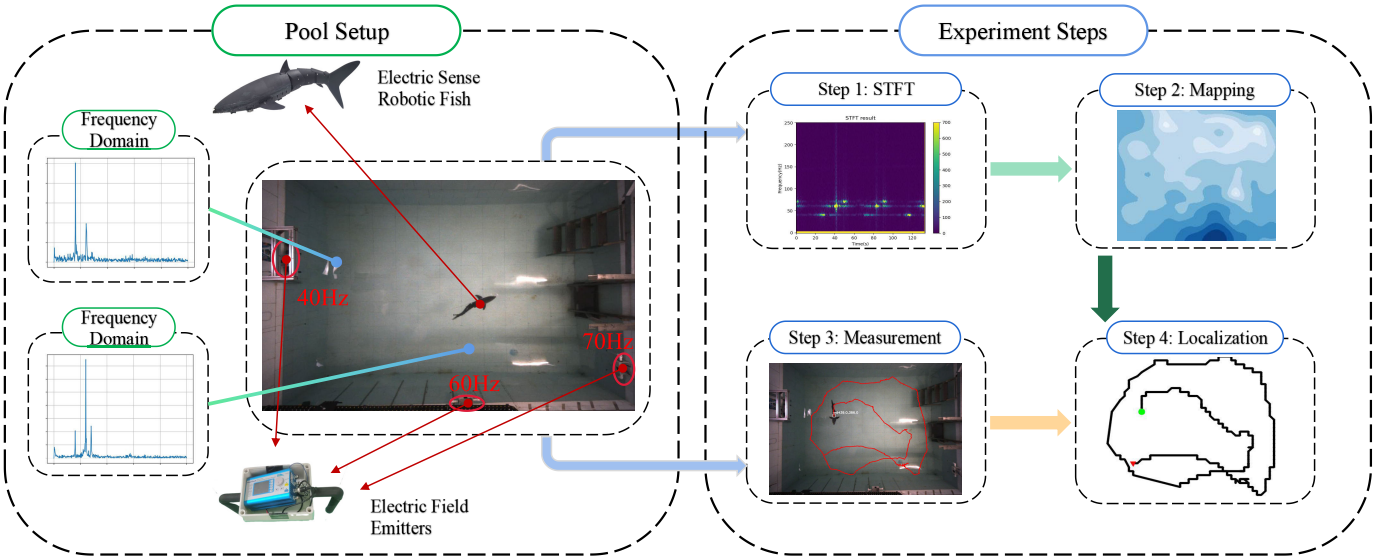

Fig. 6. General framework of our experiment. The arrows represent the flow of data. There are three electric field emitters placed in the pool, and in the different positions, the frequency domain from the robotic fish measurements has changed significantly. In step 1, the measurement data are conducted STFT in the upper computer and record amplitudes whose frequencies exhibit significant variations. In step 2, mapping the electric field maps. In step 3, underwater robot swim and measure in new trajectory. In step 4, utilize the electric field maps generated to estimate the robot's location in step 3.

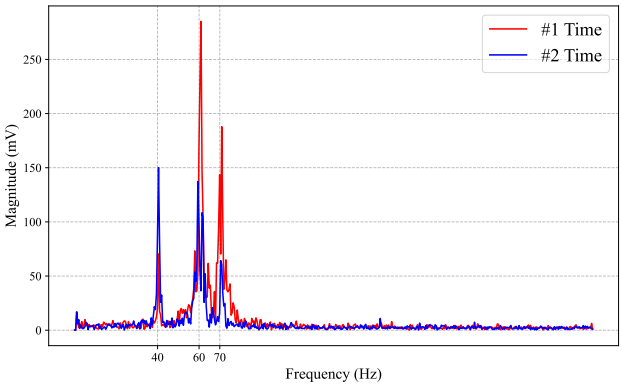

Fig. 7. Frequency domain of measurements obtained at two different times from robotic fish. There are large variations at 40, 60, and 70 Hz.

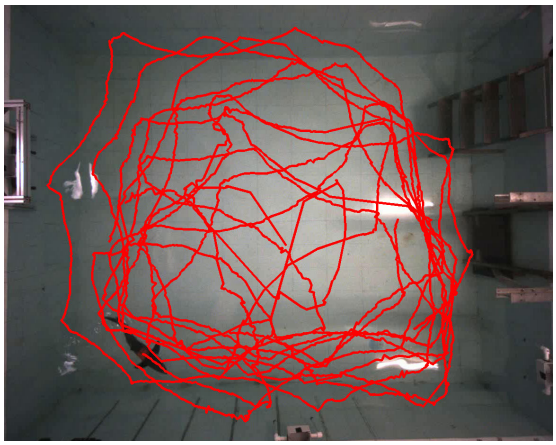

Fig. 8. Training freely swimming path (red) that is used in the mapping experiment.

Fig. 10 shows the process and result of particle filter for robot localization using a single frequency, 40 Hz, electric field map ($M = 1$ in Algorithm 1). The result shows that the predicted roughly matches the referenced trajectory. At the onset of prediction, particles are dispersed throughout the prediction space. As the iterations progress, these particles gradually converge toward a singular point. Prior to convergence, there exists notable disparity between the predicted and the actual trajectory, which can be seen in Fig. 10(b). The localization algorithm lacks knowledge of the robot's initial position, resulting in imprecise and random estimated positions prior to converge. As the particles converge, the estimating backward positions begin to correct the previous trajectory. In Fig. 10, we also show the predicted positions without estimating backward positions by yellow dashed lines. Before the particles converge, the predicted positions are very confusing due to the lack of an initial position for the robot. However, postconvergence, the predicted trajectory closely aligns with the reference trajectory. The adjustments we incorporated have enhanced the performance for predicting complete positions in the path. Fig. 10 demonstrates the convergence process and localization result of robot. In order to express the accuracy of our predictions, we employ error can be expressed as follows:

$$\text{error} = \frac{\sum_{t=0}^{n} \sqrt{(x_t - x_t^*)^2 + (y_t - y_t^*)^2}}{\text{Total Distance}} \tag{16}$$

where (x_t, y_t) is the real position in t time, and (x_t^*, y_t^*) is the predicted position. In experimental results, the errors of localization task are 0.1615 without estimating backward positions and 0.1094 with estimating backward positions, that the estimating backward positions steps effectively reduce robot localization errors. Similarly, more experiments are conducted using single electric field maps at different frequencies. When using only 60 Hz electric field map, the errors are 0.1778 without estimating backward positions and 0.1094 with estimating backward positions. Besides, for 70 Hz electric field map, the errors are 0.1463 and 0.1094 corresponding to the above introduction.

In our previous analysis, the emitters of different frequencies are considered as different landmarks. In Fig. 10, only one electric field map (40 Hz) is used for the localization

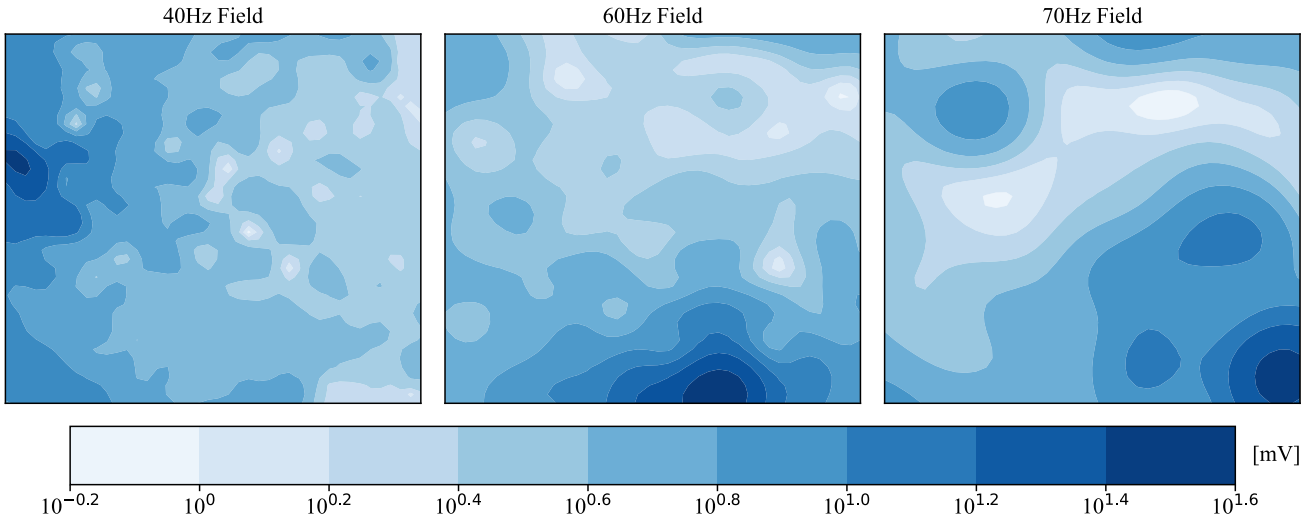

Fig. 9. Electric field mapping results. There are three electric field maps at different frequencies. The colors in these maps are represented using logarithmized measurement data.

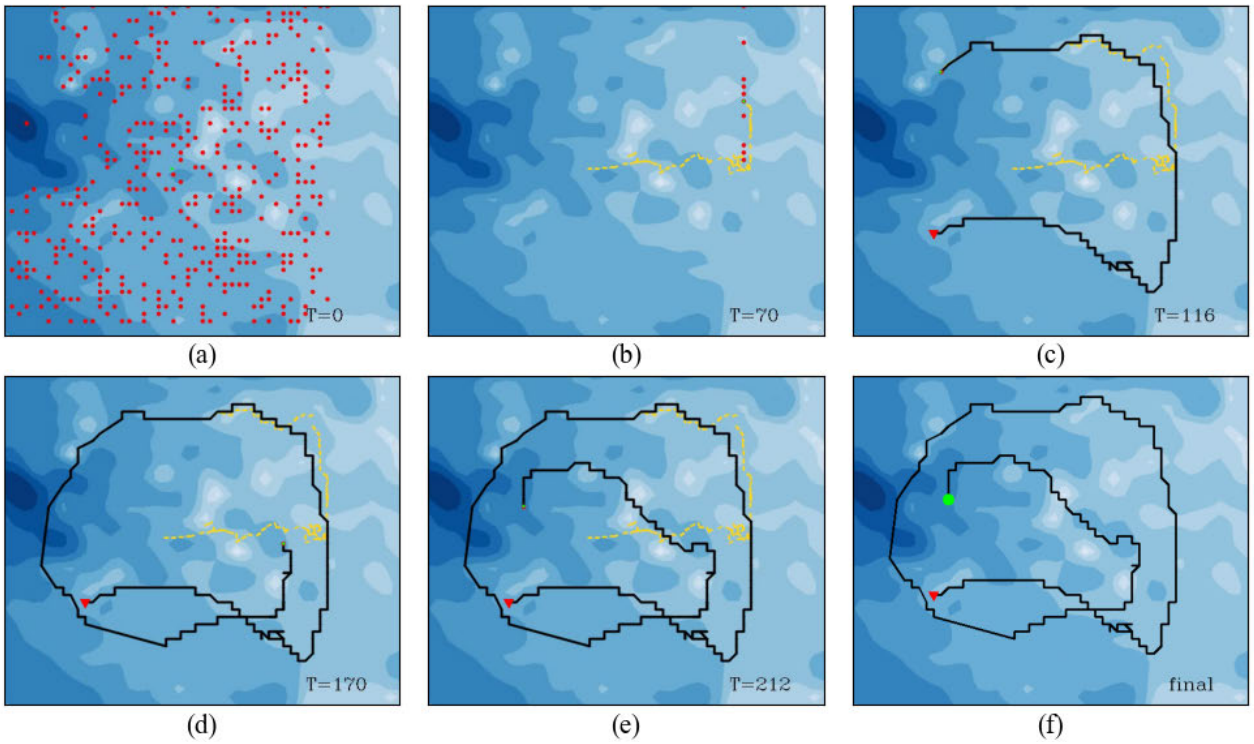

Fig. 10. Process of underwater robot localization algorithm. The yellow dashed lines indicate predicted path not corrected by estimating backward positions, and the black lines indicate correct predicted path. The red dots indicate particles. All background of the images are electric field maps for localization using only 40 Hz electric field maps. (a) Begin of algorithm. (b) Gradually converging time. (c) Converging time. (d) Localization effect after convergence. (e) Localization result. (f) Result of prediction. The red triangle is the starting point, and the green circle is the endpoint.

task. In electric theory, the electric field generated by the emitter spreads outward in surrounding manner, and its field strength forms many-to-one mapping with positions on the map, affecting the accuracy of robot localization. When more electric field emitters are used, it is equivalent to increasing the dimensions of perception data.

To illustrate the impact of multiple maps on localization accuracy, we incorporate more frequency electric field maps into the localization algorithm in the measurement trajectory shown in Fig. 11. In the picture, the black lines indicate the prediction corrected by estimating backward positions, and the yellow dashed lines as the original trajectory, with the moment of convergence of the algorithm labeled in the figure. Corresponding to the tasks in Fig. 11, Table I indicates the error to each task. For each result, at the beginning the predictions (yellow dashed lines) are very confusing since the initial position of the robot is unknown. However, as the algorithm proceeds, prediction gradually approaches the true position. In our results, using more maps improves the accuracy of the predictions, even if this improvement is small. It is worth mentioning that for both tasks, adding more maps also has an effect on the convergence process of the algorithm. For 1-task, the algorithm convergence time is halved when the number of maps used is increased to three. For 2-task, the unconverged

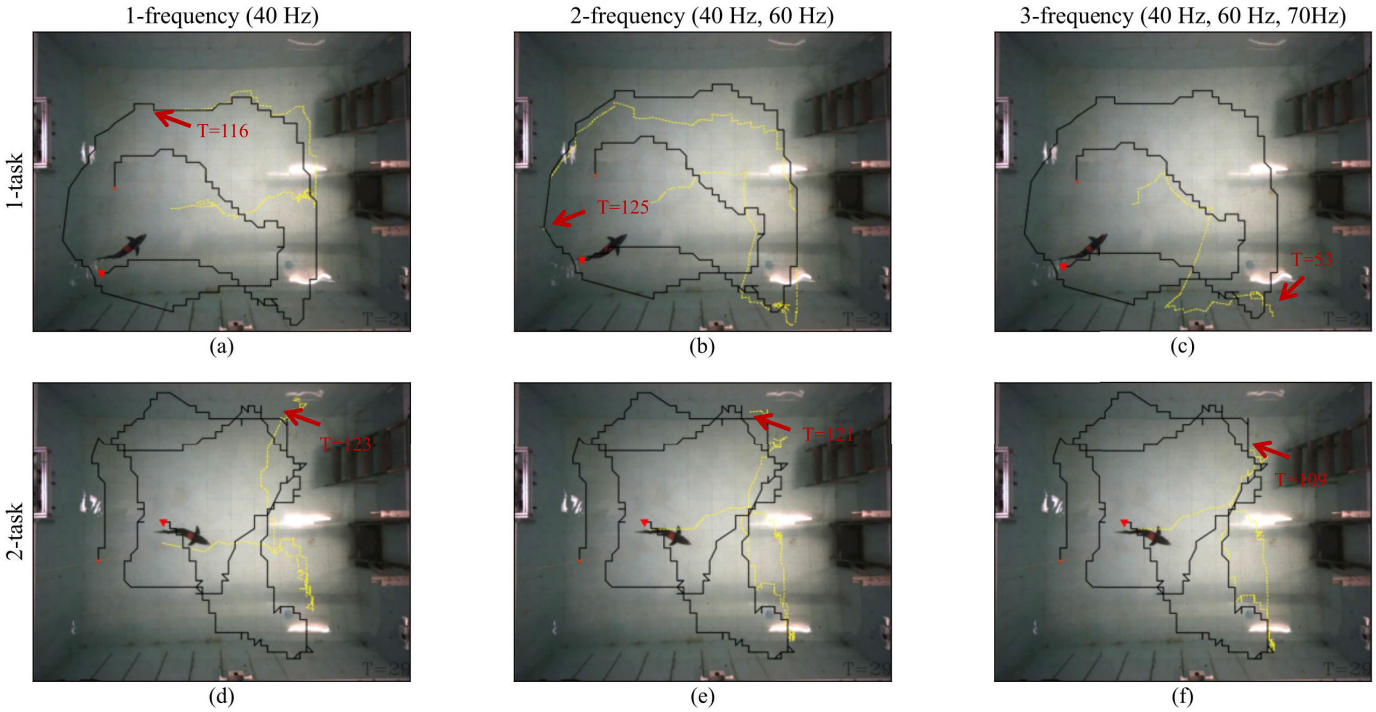

Fig. 11. Localization results of different task and multiple frequency electric field maps. The black lines are predicted results with estimating backward positions, and yellow dashed lines indicate predicted results not corrected by estimating backward positions. In each result, the convergence moment of algorithm is indicated with red arrow. (a) One map for 1-task. (b) Two maps for 1-task. (c) Three maps for 1-task. (d) One map for 2-task. (e) Two maps for 2-task. (f) Three maps for 2-task.

TABLE I
ERRORS OF DIFFERENT TASK AND ELECTRIC MAPS OF DIFFERENT FREQUENCIES FOR LOCALIZATION

Different task	1-frequency (40 Hz)	2-frequency (40 Hz, 60 Hz)	3-frequency (40 Hz, 60 Hz, 70Hz)
Estimating original positions			
1-task	0.1615	0.1395	0.1094
2-task	0.1642	0.1279	0.1276
Estimating backward positions			
1-task	0.1094	0.0930	0.0930
2-task	0.1045	0.1014	0.1014

trajectory has a large error from the actual trajectories when one map is used, while reconverging to a position close to the true value due to detection space limitations. When additional maps are added, the phenomenon is no longer occurred, that the more maps used improve the predicted accuracy. Then, the speed of convergence is marginally increased when adding maps to three in 2-task.

D. Discussion

In conclusion, our underwater robot localization algorithm for electric field maps has achieved ideal results, even when using only a map function that is not injective. According to our analysis and localization results, increasing the number of electric field maps used can provide small improvement in the accuracy and convergence speed of the localization algorithm. In order to obtain wider applications, it is meaningful to evaluate the performance of proposed methods and discuss the potential applications.

A meaningful metric is the program execution time of proposed methods. The programs involved in this work include electric field mapping and localization. For mapping program, the time spending is related to the amount of dataset, and it is mentioned in Section V-B that 148.3335 s are spent. Then for localization program, the evaluation of execution time involves using different numbers of electric field maps, which are shown in Fig. 12. When only one map is used, each step takes about 0.005 s to execute. As more maps are used, the calculation involved also increases, and the execution time of a single step exceeds 0.01 s. Using more maps requires more single-step execution time, but the accuracy increases, and the speed of convergence increases significantly, especially when using three maps. In the previous localization error analysis, using only one map can achieve good effect, and the time spending is also low. In order to improve the accuracy, it is available to increase the number of electric field maps used for localization, but this sacrifices more time to execute program.

This work mainly uses freely swimming robotic fish equipped with passive electric field sense system to explore and utilize unknown underwater electric field. Due to the particularity of underwater environment, an available underwater perception methods are currently scarce. And the proposed methods provide a framework of processing electric field data, it is hopeful to show some potentials of underwater electric sense. To the best of our knowledge, there have been studies using underwater robots to collect electric field information in the ocean [39], [40]. Through the mapping method proposed in this work, it is possible method to process these data from nature, then the underwater electric field information can be completely extracted by maps. The maps are potential for more applications, such as learning about minerals from electric field maps throughout the region. The obtained electric field maps can be applied to the proposed localization method. Based on the mapping then localization framework by passive electric

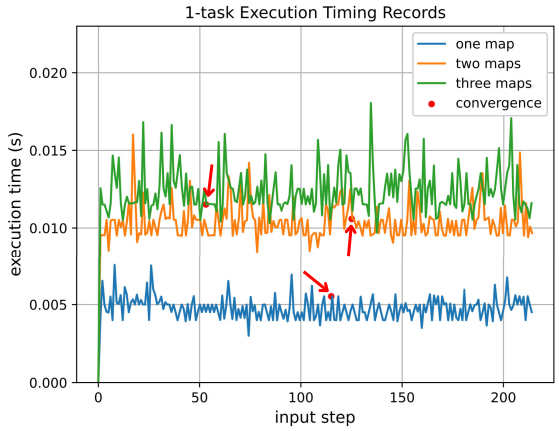

Fig. 12. Localization program execution timing records. There are three different numbers of maps execution times, which are corresponding to the 1-task in the experiment. And the red arrows indicate the convergence steps.

field sensing system, the perception method of underwater robot is probably expanded.

VI. Conclusion and Future Work

In this article, inspired by the electroreception of natural fish, we propose a passive electric sense system for robotic fish. To the best of our knowledge, previous works on underwater electric field sense have paid little attention to freely swimming underwater robots and can only be applied when the source information of the electric field is available. To address this issue, we have analyzed the characteristics of underwater electric fields by Maxwell's equations which is suitable for all electromagnetic fields. Then, an interpolation method incorporating the prior physical knowledge of underwater electric field is derived as a mapping method. By underwater electric field mapping, robot is able to obtain the underwater electric field information. Finally, we present an localization algorithm using electric field maps. Experimental results show that using the generated electric field maps, our localization algorithm achieves the desired results. The main contribution of this article is to expand the application scenarios to environments with unknown prior information about electric field sources.

In the future, our focus will be expanding application scenarios, expanding 2-D maps into 3-D maps. In addition, the computational complexity of mapping method of higher dimension needs to be further optimized to achieve faster mapping speed and better accuracy.

References

[1] R. Miao, J. Qian, Y. Song, R. Ying, and P. Liu, "UniVIO: Unified direct and feature-based underwater stereo visual-inertial odometry," *IEEE Trans. Instrum. Meas.*, vol. 71, pp. 1–14, 2022.

[2] Y. Ling et al., "Underwater tightly coupled state estimation method using IMU and artificial lateral line systems," *IEEE Trans. Instrum. Meas.*, vol. 73, pp. 1–9, 2024.

[3] J. R. Solberg, K. M. Lynch, and M. A. MacIver, "Active electrolocation for underwater target localization," *Int. J. Robot. Res.*, vol. 27, no. 5, pp. 529–548, May 2008.

[4] D. Q. Huy, N. Sadjoli, A. B. Azam, B. Elhadidi, Y. Cai, and G. Seet, "Object perception in underwater environments: A survey on sensors and sensing methodologies," *Ocean Eng.*, vol. 267, Jan. 2023, Art. no. 113202. [Online]. Available: https://www.sciencedirect.com/science/article/pii/S0029801822024854

[5] Y. Ou, J. Fan, C. Zhou, S. Tian, L. Cheng, and M. Tan, "Binocular structured light 3-D reconstruction system for low-light underwater environments: Design, modeling, and laser-based calibration," *IEEE Trans. Instrum. Meas.*, vol. 72, pp. 1–14, 2023.

[6] P. Moller, *Electric Fishes: History and Behavior*. New York, NY, USA: Chapman & Hall, 1995.

[7] A. A. Caputi, "The bioinspiring potential of weakly electric fish," *Bioinspiration Biomimetics*, vol. 12, no. 2, Feb. 2017, Art. no. 025004.

[8] F. Pedraja and N. B. Sawtell, "Collective sensing in electric fish," *Nature*, vol. 628, no. 8006, pp. 139–144, Apr. 2024.

[9] R. Murray, "Electrical sensitivity of the ampullae of lorenzini," *Nature*, vol. 187, no. 4741, p. 957, 1960.

[10] S. Lanneau, F. Boyer, V. Lebastard, and S. Bazeille, "Model based estimation of ellipsoidal object using artificial electric sense," *Int. J. Robot. Res.*, vol. 36, no. 9, pp. 1022–1041, Aug. 2017.

[11] F. Boyer, V. Lebastard, C. Chevallereau, and N. Servagent, "Underwater reflex navigation in confined environment based on electric sense," *IEEE Trans. Robot.*, vol. 29, no. 4, pp. 945–956, Aug. 2013.

[12] V. Lebastard, C. Chevallereau, A. Girin, N. Servagent, P.-B. Gossiaux, and F. Boyer, "Environment reconstruction and navigation with electric sense based on a Kalman filter," *Int. J. Robot. Res.*, vol. 32, no. 2, pp. 172–188, Feb. 2013.

[13] F. Boyer, V. Lebastard, C. Chevallereau, S. Mintchev, and C. Stefanini, "Underwater navigation based on passive electric sense: New perspectives for underwater docking," *Int. J. Robot. Res.*, vol. 34, no. 9, pp. 1228–1250, Aug. 2015.

[14] J. Zheng, C. Huntrakul, X. Guo, C. Wang, and G. Xie, "Electric sense based pose estimation and localization for small underwater robots," *IEEE Robot. Autom. Lett.*, vol. 7, no. 2, pp. 2835–2842, Apr. 2022.

[15] J. Zheng, J. Wang, X. Guo, C. Huntrakul, C. Wang, and G. Xie, "Biomimetic electric sense-based localization: A solution for small underwater robots in a large-scale environment," *IEEE Robot. Autom. Mag.*, vol. 29, no. 4, pp. 50–65, Dec. 2022.

[16] R. Safipour, S. Hölz, J. Halbach, M. Jegen, S. Petersen, and A. Swidinsky, "A self-potential investigation of submarine massive sulfides: Palinuro seamount, Tyrrhenian Sea," *Geophysics*, vol. 82, no. 6, pp. A51–A56, Nov. 2017.

[17] H. Peng, G. Shen-guang, and B. Zhong-Hua, "Detection of line spectrum of the ship shaft-rate electric field based on the improved adaptive line enhancement," in *Proc. Int. Conf. Consum. Electron., Commun. Netw. (CECNet)*, Apr. 2011, pp. 256–259.

[18] L. Shi, R. Zheng, S. Zhang, and M. Liu, "Cooperative estimation to reconstruct the parametric flow field using multiple AUVs," *IEEE Trans. Instrum. Meas.*, vol. 70, pp. 1–10, 2021.

[19] M. Seeger, "Gaussian processes for machine learning," *Int. J. Neural Syst.*, vol. 14, no. 2, pp. 69–106, 2004.

[20] F. Mackay, R. Marchand, and K. Kabin, "Divergence-free magnetic field interpolation and charged particle trajectory integration," *J. Geophys. Res., Space Phys.*, vol. 111, no. 6, pp. 1–8, Jun. 2006.

[21] H. Wu and X. Lu, "Data assimilation of high-latitude electric fields: Extension of a multi-resolution Gaussian process model (Lattice Kriging) to vector fields," *Space Weather*, vol. 20, no. 1, p. 2021, Jan. 2022.

[22] N. Wahlström, M. Kok, T. B. Schön, and F. Gustafsson, "Modeling magnetic fields using Gaussian processes," in *Proc. IEEE Int. Conf. Acoust., Speech Signal Process.*, May 2013, pp. 3522–3526.

[23] H. Liu, H. Xue, L. Zhao, D. Chen, Z. Peng, and G. Zhang, "MagLoc-AR: Magnetic-based localization for visual-free augmented reality in large-scale indoor environments," *IEEE Trans. Vis. Comput. Graph.*, vol. 29, no. 11, pp. 4383–4393, Nov. 2023.

[24] H. Momma and T. Tsuchiya, "Underwater communication by electric current," in *Proc. OCEANS*, 1976, pp. 631–636.

[25] D. Fleisch, *A Student's Guide To Maxwell's Equations*. Cambridge, U.K.: Cambridge Univ. Press, 2008.

[26] M. A. Álvarez, L. Rosasco, and N. D. Lawrence, *Kernels for Vector-Valued Functions: A Review*. Boston, MA, USA: Now, 2012.

[27] A. Solin, M. Kok, N. Wahlström, T. B. Schön, and S. Särkkä, "Modeling and interpolation of the ambient magnetic field by Gaussian processes," *IEEE Trans. Robot.*, vol. 34, no. 4, pp. 1112–1127, Aug. 2018.

[28] I. Macêdo and R. Castro, "Learning divergence-free and curl-free vector fields with matrix-valued kernels," Instituto de Matematica Pura e Aplicada, Rio de Janeiro, RJ, USA, Tech. Rep., 2010.

[29] B. Zhang, D. Ji, S. Liu, X. Zhu, and W. Xu, "Autonomous underwater vehicle navigation: A review," *Ocean Eng.*, vol. 273, Feb. 2023, Art. no. 113861. [Online]. Available: https://www.sciencedirect.com/science/article/pii/S0029801823002457

[30] C. Cadena et al., "Past, present, and future of simultaneous localization and mapping: Toward the robust-perception age," *IEEE Trans. Robot.*, vol. 32, no. 6, pp. 1309–1332, Jun. 2016.
[31] F. Gustafsson, "Particle filter theory and practice with positioning applications," *IEEE Aerosp. Electron. Syst. Mag.*, vol. 25, no. 7, pp. 53–82, Jul. 2010.
[32] S. Thrun, "Probabilistic robotics," *Commun. ACM*, vol. 45, no. 3, pp. 52–57, 2002.
[33] D. Fox, S. Thrun, W. Burgard, and F. Dellaert, "Particle filters for mobile robot localization," in *Sequential Monte Carlo Methods in Practice*. Cham, Switzerland: Springer, 2001, pp. 401–428.
[34] T. Li, M. Bolic, and P. M. Djuric, "Resampling methods for particle filtering: Classification, implementation, and strategies," *IEEE Signal Process. Mag.*, vol. 32, no. 3, pp. 70–86, May 2015.
[35] F. Chen, D. Li, C. Chen, and Y. Feng, "The detection performance of sensor on corrosion electric field of ships," in *Proc. Int. Symp. Adv. Electr., Electron. Comput. Eng.*, 2016, pp. 20–23, doi: 10.2991/isaeece-16.2016.4.
[36] K. M. Shafeeq, S. Nair, G. Uma, and T. Mukundan, "Fabrication of Ag/AgCl electrode for detection of electric field in marine environment," *IOP Conf. Ser., Mater. Sci. Eng.*, vol. 561, no. 1, Oct. 2019, Art. no. 012054.
[37] S. R. Qualls et al., "Underwater electric potential measurements using AUVs," in *Proc. OCEANS-MTS/IEEE Washington*, Oct. 2015, pp. 1–4.
[38] G. Li et al., "Towards emerging EEG applications: A novel printable flexible Ag/AgCl dry electrode array for robust recording of EEG signals at forehead sites," *J. Neural Eng.*, vol. 17, no. 2, Mar. 2020, Art. no. 026001.
[39] B. Claus, K. Weitemeyer, P. Kowalczyk, A. Proctor, C. Donald, and M. Kowalczyk, "Autonomous underwater vehicle based electric and magnetic field measurements with applications to geophysical surveying and subsea structure inspection," in *Proc. IEEE/OES Auto. Underwater Vehicles Symp. (AUV)*, Sep. 2020, pp. 1–5.
[40] Z. Zhu et al., "Autonomous-underwater-vehicle-based marine multicomponent self-potential method: Observation scheme and navigational correction," *Geosci. Instrum., Methods Data Syst.*, vol. 10, no. 1, pp. 35–43, Feb. 2021.

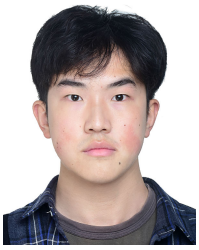

Penghang Shuai received the B.E. degree in electrical engineering and automation from the College of Nuclear Technology and Automation Engineering, Chengdu University of Technology, Chengdu, China, in 2018. He is currently pursuing the M.E. degree in artificial intelligence with the Institute of Automation, Chinese Academy of Sciences, Beijing, China.

His research interests include underwater robotics and electric field sense.

Haipeng Li received the B.E. degree in mechatronics from Qilu University of Technology, Jinan, China, in July 2000, and the Ph.D. degree in vehicle engineering from the University of Science and Technology Beijing, Beijing, China, in 2006.

He is currently a Professor with the Laboratory of Cognition and Decision Intelligence for Complex Systems, Institute of Automation, Chinese Academy of Sciences (IACAS). His current research interests in the underwater biomimetic robot.

Chao Zhou (Senior Member, IEEE) received the B.E. degree in automation from Southeast University, Nanjing, China, in July 2003, and the Ph.D. degree in control theory and control engineering from the Institute of Automation, Chinese Academy of Sciences (IACAS), Beijing, China, in 2008.

He is currently a Professor with the Laboratory of Cognition and Decision Intelligence for Complex Systems, IACAS. His current research interests include the motion control of robot, the bioinspired robotic fish, and embedded system of robot.

Yaming Ou (Graduate Student Member, IEEE) received the B.E. degree in automation from Southeast University, Nanjing, China, in 2021. He is currently pursuing the Ph.D. degree in control theory and control engineering with the Institute of Automation, Chinese Academy of Sciences (IACAS), Beijing, China.

His research interests include underwater 3-D vision, SLAM, multisensor fusion, and autonomous robot navigation.

Zhuoliang Zhang received the B.E. degree in automation from Tongji University, Shanghai, China, in July 2018, and the Ph.D. degree in control theory and control engineering from the Institute of Automation, Chinese Academy of Sciences (IACAS), Beijing, China, in June 2023.

He is currently a Post-Doctoral FELLOW with the Laboratory of Cognition and Decision Intelligence for Complex Systems, IACAS. His research interests include measurements, sensor signal processing, and intelligent control.

Chunhui Zhu received the B.E. degree in data science from Peking University, Beijing China, in 2020. He is currently pursuing the Ph.D. degree in control theory and control engineering from the Institute of Automation, Chinese Academy of Sciences, Beijing, China.

His current research interests include robotic fish, soft robot, and robot motion control.

Junfeng Fan (Senior Member, IEEE) received the B.S. degree in mechanical engineering and automation from Beijing Institute of Technology, Beijing, China, in 2014, and the Ph.D. degree in control theory and control engineering from the Institute of Automation, Chinese Academy of Sciences (IACAS), Beijing, in 2019.

He is currently an Associate Professor of Control Theory and Control Engineering with the State Key Laboratory of Management and Control for Complex Systems, IACAS. His research interests include robot vision and underwater robot.